More than a Liquid Junction: Effect of Stirring, Flow Rate, and Inward and Outward Electrolyte Diffusion on Reference Electrodes with Salt Bridges Contained in Nanoporous Glass

Evan L. Anderson,[†] Timothy P. Lodge,[†,‡] Tata Gopinath,[‖] Gianluigi Veglia,[†,‖] and Philippe Bühlmann*[,†]

† *Department of Chemistry,* ‡ *Department of Chemical Engineering & Materials Science, and* ‖ *Department of Biochemistry, Molecular Biology, & Biophysics, University of Minnesota, Minneapolis, MN 55455-0431*

* *corresponding author: Philippe Bühlmann, buhlmann@umn.edu*

ABSTRACT

The Henderson equation is usually used to calculate liquid junction potentials between miscible electrolyte solutions. However, the potentials of reference electrodes that comprise an electrolyte-filled nanoporous glass frit may also be affected by charge screening. As reported previously, when the Debye length approaches or surpasses that of the glass pore diameter, reference potentials depend on the composition of the bridge electrolyte, the pore size of the frit, and the concentration of electrolyte in the sample. We report here that stirring of samples may alter the reference potential as it affects the electrolyte concentration in the section of the nanoporous glass frits that is facing the sample solution. When the flow rate of bridge electrolyte into the sample is small, convective mass transport of sample into the nanoporous frit occurs. The depth of penetration into the frits is only a few nanometers but, despite the use of concentrated salt bridges, this is enough to affect the extent of electrostatic screening when samples of low ionic strength are measured. Mixing of sample and salt bridge solutions—and in particular penetration of sample components into the frit—was optically monitored by observation of a deeply colored $Fe[(SCN)(H_2O)_5]^{2+}$ complex that formed in situ exclusively in the region where the sample and salt bridge mixed. Importantly, because flow through nanoporous frits is very slow, mass transport through these frits is dominated by diffusion. Consequently, over as little as one hour, reference electrode frits with low flow rates become contaminated with sample components and undergo depletion of electrolyte within the frit to a depth of several millimeters, which can negatively affect subsequent experiments.

KEYWORDS: Reference electrode, salt bridge, liquid junction, nanoporous glass, stirring effects, Vycor, solid-state NMR

INTRODUCTION

A range of advances in the design of reference electrodes have been made over the past decades and provide important improvements toward calibration-free electrochemical sensing[1] and long-term measurements.[2] They include the use of nanoporous glasses with various pore sizes,[3] ionic liquid salt bridges,[4-6] and solid state designs.[7-12] Most designs have a particular application in mind, such as the flexible reference electrodes that enable wearable sensors[13-14] or paper-based devices,[15] and as a result they have each their own unique advantages. However, even though innovation in this field has allowed overcoming problems encountered in specialized applications, the use of reference electrodes that comprise a free-flowing liquid junction or a liquid junction in which flow is restrained by porous glass, ceramic materials, or capillaries is still widespread and appears unlikely to disappear any time soon. Unfortunately, the limitations of these junctions are cause of many errors and much loss of time in routine analysis.[16] Surprisingly, only little attention has been given in the past to the effect on reference potentials of seemingly obvious experimental parameters such as stirring and bridge electrolyte flow.

Reference electrodes with free-flowing liquid junctions[17] were shown to provide stable reference potentials, where, with some assumptions, the liquid-junction potential can be calculated theoretically.[18-22] Here we apply the Henderson equation to do so.[22] The use of free-flowing liquid junctions, however, requires that the bridge electrolyte be refilled regularly. To reduce maintenance, the loss of bridge electrolyte can be slowed by placing a capillary or porous frit between the bridge electrolyte and sample (using frits with pore diameters of 5 – 1000 nm)[3] or by stopping the flow of bridge electrolyte altogether with a gel.[23] This reduces maintenance but can lead to new problems, such as contamination or depletion of the bridge electrode within the frit if flow rates are low. This results, e.g., in slow responses of combination pH electrodes after exposure to samples with a low electrolyte content for long periods of time, a problem frequently encountered in routine analysis and often misinterpreted as a slow response of the pH sensitive

half cell. To avoid problems associated with low flow rates, pressurized inner filling solutions have been applied to ensure a continuous flow of electrolyte through the restrained liquid junction.[24-30]

Of the restrained liquid junctions, the most commonly used reference electrode design contains a micro- or nanoporous frit that separates the sample from an inner filling solution (typically composed of concentrated KCl) that contacts a AgCl-coated Ag wire. The phase boundary potential across the interface of the inner filling solution and AgCl/Ag depends on the activity of Cl^-, as defined by the Nernst equation.[31] As the inner filling solution is separated from the sample by the porous frit/salt bridge, this KCl|AgCl|Ag phase boundary potential is not affected by the sample. It is usually assumed that the interface between the electrolyte-filled porous frit and the sample solution contributes with a liquid junction potential, the size of which can be predicted quantitatively.[22] However, it has been shown that charge screening caused by the negative charges on the pore walls at the interface of nanoporous glass frits and sample solutions may result in phase boundary potentials that differs from the liquid-junction potential predicted for a free-flowing junction.[3, 32] The extent of charge screening depends on the pore size and composition of the frit material as well as the electrolyte strength and pH of the sample solution.[3] As the ionic strength of sample solutions is decreased, the Debye length in these solution approaches and eventually surpasses that of the frit pore size, resulting in charge screening (see Figure 1).[33]

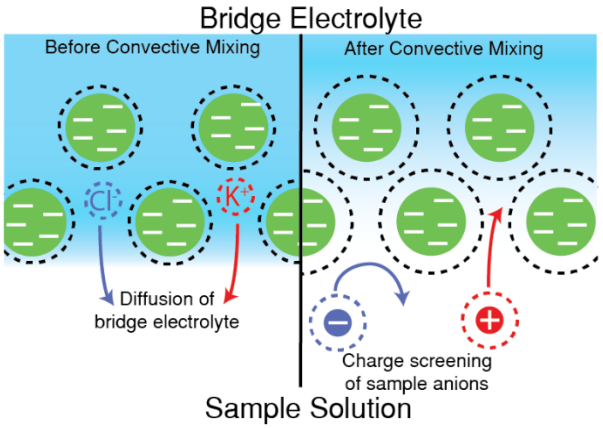

Figure 1. Charge screening at the interface of a porous frit filled with bridge electrolyte and a sample solution. Dotted lines represent the thickness of the Debye layer, which prevents anions

from entering the porous matrix. Pore walls represented as circles, a simplification used for the calculations described in the section Stirred Regions within Nanoporous Frits.

In this contribution we show that stirring of sample solutions may affect reference potentials, an effect that has been ignored in the prior literature on porous liquid junctions. We constructed electrochemical cells to determine the potential of cells comprising nanoporous glass frits in stirred/laminar flow solutions and unstirred solutions. Moreover, the extent to which stirred regions penetrate into nanoporous glass was assessed using a simple hydrodynamic scaling model.[34-36] Convection within a thin frit section that is nearest to the sample leads to mixing of the sample solution with the salt bridge electrolyte. This can alter the Debye length of the solution within the frit and affects charge screening by the negatively charged pore walls. To describe this process, the flow rate of reference electrodes was compared in this work with the distance K^+ and Cl^- ions diffuse through the frit over a comparable timespan. This work shows that diffusion is the dominant process in reference electrodes with 2.0–5.5 nm pores, allowing for electrolyte to diffuse both out of and into the reference electrodes. Diffusion was also qualitatively studied by visually monitoring mixing of $FeCl_3$ and KSCN solutions.[17] The dark red complex $Fe[(SCN)(H_2O)_5]^{2+}$ forms where the Fe^{3+} and SCN^- containing solutions mix,[37] visualizing the location of the diffusional fronts within frits. Images that show time-dependent mixing within nanoporous frits highlight the significant contamination of nanoporous frits in the course of electrochemical measurements.

EXPERIMENTAL SECTION

Materials

AgCl (98%), KCl, $FeCl_3$, sodium acetate-$^{13}C_2$, LiOH, Dowex HCR-W2, and 1.0 M HCl were purchased from Sigma-Aldrich, Ag wires (0.5 mm diameter, ≥ 99.9%) from Alfa Aesar, porous Vycor glass frits (28% pore volume, 2.0–5.5 nm pore diameter, 3 mm diameter, 3 mm length, 1.5 g/cm^3 density, and 250 m^2/g surface area)[38-39] from Bioanalytical Systems, a pH glass electrode

from Hanna Instruments, and KSCN from J.T. Baker Chemical Corporation. All chemicals were used as received.

Preparation of AgCl-coated Ag wires

Ag wires were cleaned in 3 M nitric acid for 30 s and rinsed using deionized purified water. Wires were then placed in 0.1.0 M HCl with a Pt mesh counter electrode and a Ag/AgCl (3M KCl) reference electrode equipped with a Vycor frit. A current of 0.4 mA/cm^2 was applied for 45 min. The AgCl-coated wires were cleaned with deionized water and allowed to age for at least 24 h in AgCl-saturated H_2O.

Preparation of Porous Frit Reference Electrodes for Electrochemical Measurements

Vycor frits were cleaned in stirred deionized water at 60 °C for 6 h. This process was repeated three times before drying of the frits under vacuum. Vycor frits were attached to glass tubes (5 cm long, 3 mm diameter) with Teflon heat shrink tube. The glass tubes were then filled with 3 M KCl saturated with AgCl and stored in 3 M KCl for at least two days prior to measurements. The height of the inner filling solution was 5 cm, which generated a constant pressure of 5×10^{-3} bar and flow rate of 4 ± 2 nL/h.[3] AgCl/Ag wires were inserted through rubber septa into the glass tubes before measurements.

Potentiometric Measurements

A Lawson Labs EMF 16 channel potentiometer (Malvern, PA) controlled by EMF Suite 1.02 software was used for all measurements of potentials (*E*). Each measurement was performed at room temperature (23 ± 2 °C). KCl solutions were prepared by serial dilution with purified water (18.2 MΩ cm specific resistance, EMD Millipore, Philadelphia, PA) from 1.0 M KCl stock solutions. Potentials were measured relative to a Mettler Toledo DX200 free-flowing double junction reference electrode (with a 3.0 M KCl bridge electrolyte and AgCl-saturated 3.0 M KCl inner reference electrolyte).[17] A schematic of the experimental setup is included in the Supplemental Information (Figure 2). The tubular electrode bodies were not sealed at the top to allow for gravity driven solution flow towards the samples. Activity coefficients were calculated

using a two-parameter Debye-Hückel approximation,[33] and all potential measurements were corrected for liquid junction potentials at the free-flowing double junction reference electrode using the Henderson equation.[18] Alternative methods for the calculation of liquid-junction potentials are available, but for most cases predictions from different models differ only slightly (see ref. 22 for more information).

A Corning PC-420D hot plate was used for stirring. Stirred solutions corresponded to a magnetic stir bar rotation rate of 400 rotations per minute. A 150 mL glass beaker (55 × 85 cm) with a 1 × 6.4 mm Teflon-coated cylindrical stir bar was used for all potentiometric measurements. The reference electrode comprising the Vycor frit was immersed into the sample solutions to a depth of 1 cm.

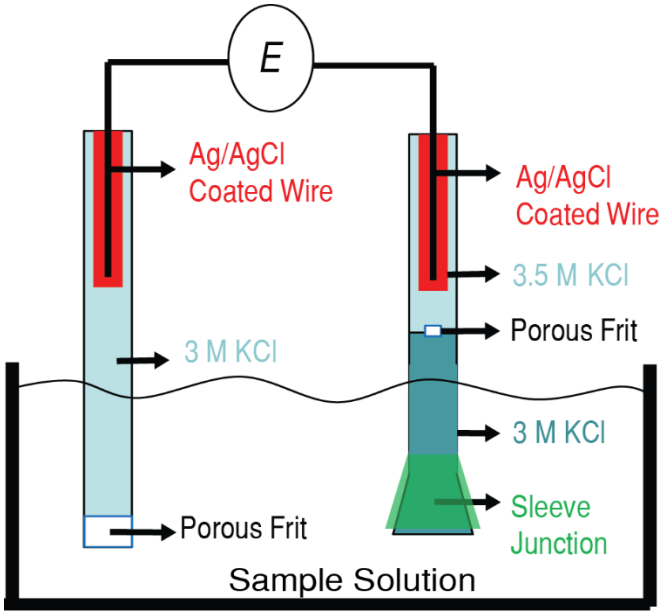

Figure 2. Schematic of the experimental setup used to measure potentials at the interface of sample solutions and porous frits.

Resistance Measurements

Resistances were measured with the known shunt method.[40] The potentials (E_1) of three porous frit reference electrodes (filled with 3 M KCl) were first measured in stirred and unstirred 100 µM LiCl solutions versus a free-flowing double junction reference electrode. The potentials

(E_2) were measured a second time after the porous frit reference electrode was shorted to the free-flowing double junction reference electrode through a 48 kΩ resistor in stirred and unstirred 100 μM LiCl solutions. Resistances were calculated as 48 kΩ × ($E_1 - E_2$) / E_2.

Preparation of Lithium Acetate-$^{13}C_2$

Dowex HCR-W2 cation-exchange resin was loaded onto a column (resin: 1.5 cm × 20 cm) and rinsed with five column volumes of 1.0 M HCl to ensure that the resin was loaded with H^+. The resin was then rinsed with purified water until the eluent reached pH = 7, as monitored with pH test strips, to ensure removal of excess HCl. Then, 1.0 M sodium acetate-$^{13}C_2$ was loaded onto the column. The acetic acid-$^{13}C_2$ resulting from the Na^+ versus H^+ ion exchange was eluted with purified water (~ 200 mL) until pH 6 was reached. A flame test was used to ensure that no Na^+ was contained in the thus obtained eluent. To do so, a small amount of eluent was placed in a natural gas flame. The bright orange color characteristic for sodium was absent. The eluent containing the acetic acid-$^{13}C_2$ was neutralized to pH 7 by addition of LiOH, as monitored with a Hanna Instruments pH glass electrode. The resulting solutions were lyophilized, and the dried lithium acetate-$^{13}C_2$ was dissolved in D_2O to give a 1.0 M solution.

Solid-State NMR of Lithium Acetate-$^{13}C_2$

^{7}Li and ^{13}C solid-state NMR spectra were acquired in the absence and presence of Vycor glass on an Agilent 700 MHz spectrometer. Vycor frits were ground using a mortar and pestle to a fine powder. The powder was suspended in 1.0 M lithium acetate-$^{13}C_2$ and tightly packed into a 3.2mm solid-state NMR rotor. An additional sample was prepared without Vycor glass powder. ^{7}Li and ^{13}C NMR spectra were acquired using static and magic angle spinning conditions using 10 kHz spinning rate. The 1D ^{7}Li and ^{13}C spectra were processed using a 100 Hz exponential multiplication function.

Preparation of Porous Frit Reference Electrodes for Visualization of Diffusion and Flow

Vycor frits were cleaned and attached to glass tubes as described above. The glass tubes were then filled with one of four solutions, i.e., 2.5 M KSCN/1.0 M KCl, 50 mM $FeCl_3$, 5 mM $FeCl_3$,

171 or 0.5 mM $FeCl_3$. Finally, the tubes were stored for at least two days in solutions identical to those
172 within the glass tubes. Freshly prepared $FeCl_3$ solutions were used at the start of each experiment
173 as changes in solution color were noted after one week. Reference electrodes filled with 2.5 M
174 KSCN/1.0 M KCl were rinsed and placed into stirred or unstirred solutions of 50, 5, or 0.5 mM
175 $FeCl_3$. Reference electrodes filled with 50, 5, or 0.5 mM $FeCl_3$ were rinsed and then placed into
176 stirred or unstirred solutions of 2.5 M KSCN/1.0 M KCl.

177 **RESULTS AND DISCUSSION**

178 **Electrode Potentials in KCl Electrolyte Solutions**

179 Reference electrodes equipped with nanoporous glass junctions were immersed into
180 aqueous KCl solutions under stirred/laminar-flow and unstirred conditions, and their half cell
181 potentials were measured relative to a reference electrode that comprised a free-flowing double
182 junction (for a schematic of the experimental setup, see Figure 2). The reference electrodes with
183 the frits with 2.0–5.5 nm pores were found to have the same reference potentials in stirred (400
184 rotations per minute) and unstirred solution when they were immersed in solutions of high ionic
185 strength (Figure 3). When solutions of lower KCl concentration were stirred with a magnetic
186 stirring bar, resulting in laminar flow conditions (◇), the potential of the reference electrodes with
187 the nanoporous glass junction depended on the KCl concentration in the sample solution, which is
188 consistent with previous reports,[3, 32] indicating that charge screening occurs at low electrolyte
189 solutions, causing potentials to develop at the nanoporous glass frit due to the negatively charged
190 frit surfaces (i.e., formation of a phase boundary potential due to partial permselectivity).[41-44]
191 Moreover, even in unstirred solutions, reference potential variations were approximately five times
192 greater than those predicted for a liquid-junction potential. As shown in Figure 4, when stirring
193 was stopped, reference potentials stabilized after ~ 2 min to values closer but not consistent with
194 those predicted for a liquid-junction potential.
195

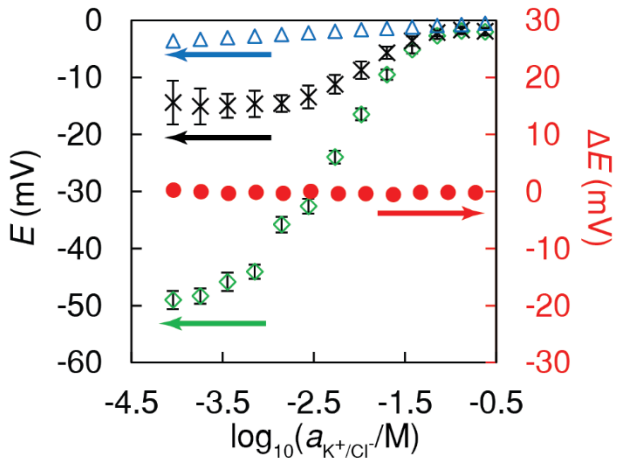

196

197 **Figure 3.** Left axis: Potentials of nanoporous frit reference electrodes as a function of the K^+/Cl^-
198 activity of a KCl solution under stirred/laminar flow (◇) and unstirred (×) conditions and of
199 calculated liquid junction potentials[18] (△) at the corresponding concentrations K^+/Cl^- activities.
200 Right axis: Difference in *E* of a AgCl/Ag wire in stirred and unstirred conditions as a function of
201 the K^+/Cl^- activity (●). *E* was measured relative to a free-flowing double-junction reference
202 electrode. *E* values of the nanoporous frit reference electrodes are corrected for liquid junction
203 potentials at the free-flowing double junction.[18] Error bars are 95% confidence intervals for the
204 average of six electrodes.

205

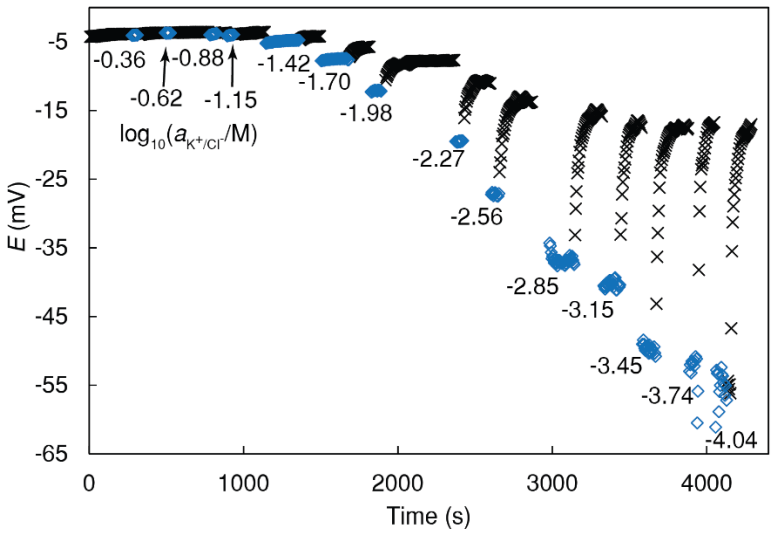

206

207 **Figure 4**. Time dependent potential of a reference electrode with a nanoporous frit as a function
208 of K^+/Cl^- activity of a KCl solution under stirred/laminar-flow (◇) and unstirred (×) conditions.
209 All *E* values are corrected for liquid junction potentials at the free-flowing double junction
210 electrode.[19] The KCl concentration was diluted stepwise by half after each stirred/unstirred
211 cycle; the numbers in the graph stand for the logarithm of the K^+/Cl^- activity.

212 In control experiments, the potential of a AgCl-coated Ag wire was measured relative to a
213 reference electrode with a free-flowing double junction to test the expectation that the reference
214 potential of the electrode with the free-flowing double junction does not differ significantly in
215 stirred and unstirred solutions. Theory predicts that the potential of a AgCl-coated Ag wire in KCl
216 solution depends on the activity of Cl^- in a Nernstian manner[45] and does not depend on the stirring
217 conditions (provided the solution is already well mixed). Indeed, the reference potential of the
218 electrode with the free-flowing double junction at each KCl concentration studied (0.8 to 9.2 ×
219 10^{-5} M KCl) differed by less than 1.0 mV between unstirred to stirred conditions, confirming that
220 the changes in potential upon stirring as shown in Figures 3 and 4 originate from the use of
221 nanoporous glass frits. In addition, the rotation rate of the magnetic stir bar also affected the
222 reference potential, with increased stir rates increasing the potential deviations (Figure S1).
223 Similarly, a dependence of the reference potential on the position of the electrode can be expected
224 if the reference electrode is moved between locations characterized by different rates and

directions of the sample flow. These results show that lateral flow at the nanoporous glass surfaces significantly affects reference potentials and must be carefully controlled when working with solutions of low electrolyte strength.

Stirred Regions within Nanoporous Frits

Multiple studies have been reported that describe the qualitative and quantitative identity of stirred areas that form within porous media in contact with stirred solutions undergoing viscous flow.[46-51] In order to approximate the depth to which these stirred regions penetrate into the porous glass network, we used a straightforward relationship between viscous flow and the depth that flow can penetrate into a porous surface section represented by spherical objects (see Figure 5). The argument is based on the classical Kirkwood-Riseman theory of hydrodynamic interactions in a "non-draining" polymer solution,[34-35] but adapted to the current problem.[36] Assuming a field of uniform spheres of radius R and total volume fraction $\emptyset$, the number density (n/V) of spheres can be calculated as:

$$\frac{n}{V} = \frac{3\,\emptyset}{4\,\pi\,R^3} \tag{1}$$

The shear force that is required for the flow to penetrate a distance L into the porous space (F_1) is calculated to be:

$$F_1 = A\,L\,\frac{n}{V}\,6\,\pi\,\eta_s\,R\,v_s \tag{2}$$

where η_s is the viscosity, v_s is the velocity of the laminar flow above the porous space, and A is the surface area of the porous material exposed to the laminar flow. Insertion of the right hand side of eqn 1 for n/V in eqn 2 gives:

$$F_1 = 4.5\,A\,L\,\emptyset\,\eta_s\,R^{-2}v_s \tag{3}$$

The shear force drop across distance L (F_2) can be calculated as:

$$F_2 = A\,\eta_s\,v_s/L \tag{4}$$

Setting F_1 equal to F_2 gives:

$$4.5\,A\,L\,\emptyset\,\eta_s\,R^{-2}v_s = A\,\eta_s\,v_s/L \tag{5}$$

Eqn 5 can be solved for L as a function of the volume fraction and pore size:

$$L = \sqrt{\frac{1}{4.5\,\emptyset}}\,R \qquad (6)$$

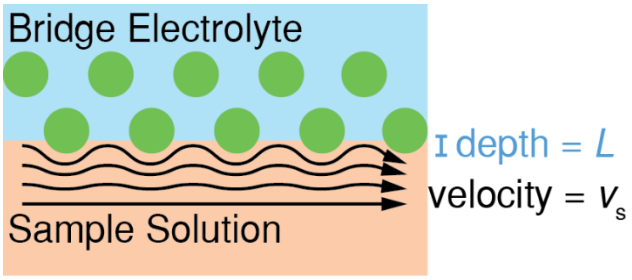

Figure 5. Schematic of a field of uniform spheres (green circles) in contact with a laminar flow (black arrows) of velocity v_s. The velocity of flow is assumed to be 0 at depth L into the porous field.

Eqn 6 predicts that the viscous flow of solution outside of a nanoporous frit with $\emptyset = 0.72$ and $R = 1.00 – 2.25$ nm will penetrate into the porous frit to a depth of order 0.56 – 1.25 nm.[38] It follows that solution flow within the few nanometers of the frit closest to the sample solution contributes to mass transport. When samples have a different ionic composition than the bridge electrolyte, this reduces the concentration of bridge electrolyte in the frit but near the interface of the sample and the porous frit. Moreover, the formation of swirls, i.e., circular flow above the curved flow lines shown in Figure 5, has been shown,[46] which may contribute to further local dilution of the bridge electrolyte. In the case of a frit filled with KCl of a high concentration and a sample solution of low ionic strength, local depletion of KCl within the frit results in an increase in the Debye length within the few nanometers of frit closest to the sample solution, increasing the extent of ionic screening by the charged pore walls.[3, 32-33] This description is further supported by resistance measurements of porous frit reference electrodes in stirred and unstirred 100 µM LiCl sample solutions. For unstirred solutions, a resistance of 40 ± 1 kΩ (95% confidence interval) was measured. For stirred solutions (400 rotations per minute), the resistance increased to 86 ± 2 kΩ (95% confidence interval), which is consistent with a significant increase in charge screening at the interface of the porous frit facing the sample due to penetration of lower ionic strength 100 µM LiCl solution into the frit.

The previously reported flow rate of nanoporous glass reference electrodes (2.0–5.5 nm pores),[3] 4 nL/h, can be converted to a linear flow rate at which solution passes through the nanoporous frit by dividing the volumetric flow rate by the fraction of the frit cross section not occupied by glass (2.8×10^{-6} m^2), resulting in 1.4×10^{-6} m/h. This flow rate is very small compared to the diffusion lengths over one hour of 3.5×10^{-3} and 3.6×10^{-3} m (calculated as the square root of 2×diffusion coefficient×time)[52] for K^+ and Cl^-, respectively, which shows that only 0.04% of the net ion transport results from solution flow and but 99.96% of the net ion transport is the result of diffusion. This indicates that the decrease the measured potential, *E,* after stirring is stopped results from the elimination of convective mass transport in the surface region of the frit, allowing for diffusion to reestablish a high concentration of the bridge electrolyte in the surface-near region of the frit, and leading to greatly decreased charge screening and a liquid junction potential that can be predicted with the Henderson equation.

Ion Adsorption to Nanoporous Frits as Observed by NMR Spectroscopy

We used magic angle spinning (MAS) solid-state NMR spectroscopy to investigate whether adsorption of electrolyte ions to the surface of the nanoporous glass is significant and, thereby, affects the overall rate of electrolyte ion transport through the frit. Since both potassium and chloride do not have isotopes readily amenable to NMR spectroscopy, we used lithium acetate instead, which is another commonly used equitransferrent electrolyte often used in salt bridges.[22, 53]

^{7}Li and ^{13}C solid-state NMR spectra acquired under static conditions with 1.0 M lithium acetate-$^{13}C_2$ ($^7Li^+$, 3.25 ppm, s; $^{13}CH_3$, 36.26 ppm, s; $^{13}COO^-$, 194.53 ppm, s) exhibited signals identical to those containing 1.0 M lithium acetate-$^{13}C_2$ in contact with ground nanoporous glass recorded with a MAS rate of 10 kHz ($^7Li^+$, 3.25 ppm, s; $^{13}CH_3$, 36.58 ppm, s; $^{13}COO^-$, 194.90, s). If more than a very small fraction of the $^7Li^+$ ions in the system had adsorbed to the glass surface, MAS spectra would be expected to either give rise to new peaks at chemical shifts characteristic for the unique chemical environment on the glass surface or, if chemical exchange between freely

dissolved and adsorbed ions were rapid, the chemical shifts observed with and without spinning would have been a weighted average between the two species. Therefore, these results show that neither lithium nor acetate ions adsorb to any significant level to the surface of the nanoporous glass. As prior work has shown only minimal differences in the effect of different electrolyte salts on charge screening,[32] we assume that potassium and chloride also do not adsorb to the nanoporous glass, an assumption that can unfortunately not be corroborated by NMR spectroscopy.

Visualization of Diffusion through Nanoporous Frits

In situ formation of the complex $Fe[(SCN)(H_2O)_5]^{2+}$ where solutions of KSCN and $FeCl_3$ meet and mix has been used previously to visualize the flow of bridge electrolyte out of reference electrodes with a free-flow design.[17] However, unlike in the original work that took advantage of this process, flow rates through the (nanoporous) frits used in this work were so low that solution flow does not explain the color formation observed in our work. As discussed above, as a mode of mass transport through nanoporous frits, diffusion dominates over hydrodynamic flow. Therefore, the color changes described below provide a qualitative visualization of the *diffusion* of ions into and out of nanoporous frits and are only minimally affected by solution flow.

The two top panels of Figure 6 show three separate reference electrodes, each filled with 2.5 M KSCN and 1.0 M KCl, exposed to unstirred 50, 5.0 and 0.5 mM solutions of $FeCl_3$. If the same solutions are mixed in a beaker, i.e., without the nanoporous frit as diffusion barrier, a dark red color is formed instantaneously. The reference electrode exposed to the 50 mM $FeCl_3$ solution showed within a few minutes a narrow stream of red color that originated at the frit surface and flowed approximately vertically downwards. The stream could be easily misinterpreted as solution flow out of the reference electrode. However, this explanation is inconsistent with the small flow of solution through the frit, as described above. Instead, diffusion of KSCN and KCl out of the frit into the less dense $FeCl_3$ solution creates locally at the interface of the frit and the solution a dense solution (colored by $Fe[(SCN)(H_2O)_5]^{2+}$) that subsequently flows downwards, driven by gravity. This stream persisted for the duration of the experiment. Diffusion of Fe^{3+} from the 50 mM $FeCl_3$

325 solution in the beaker into the frit also resulted in the formation of the dark red colored
326 $Fe[(SCN)(H_2O)_5]^{2+}$ complex in the frit, a process that within one hour nearly penetrated the height
327 of the porous frit. Note that the diffusion length of Fe^{3+} in bulk water over 1 h is 2.1×10^{-3} m,[54]
328 and Fe^{3+} diffusion through nanoporous frit is expected to be slowed down by no more than one
329 order of magnitude due to confinement.[55] Adsorption of Fe^{3+} to glass surfaces has been reported,[56]
330 but complete surface coverage (1×10^{-6} mol/m^2)[18] of the frits used for this study (surface area
331 approximately 7.9 m^2) with Fe^{3+} would result in only 7.9×10^{-6} mol of Fe^{3+} adsorbed, which is
332 less than 1% of the Fe^{3+} contained in the samples. Therefore, Fe^{3+} adsorption to glass does not
333 affect the optical assessment of solution flow through the frits.

334 A downward stream of color and the Fe^{3+} penetration into the frit still occurred as the
335 concentration of $FeCl_3$ in the sample solutions was reduced to 5.0 mM. However, for the 0.5 mM
336 $FeCl_3$ solution neither a downward stream nor coloring of the frit was observed, and only a faint
337 coloring of the $FeCl_3$ solution was detected, despite the fact that direct mixing of 0.5 mM $FeCl_3$
338 with 2.5 M KSCN and 1.0 M KCl in a beaker (i.e., in the absence of a nanoporous frit) still
339 produces a deeply red colored solution. This is consistent with partial ion screening at the
340 sample/frit interface, as also indicated by the potentiometric measurements. Notably, no
341 differences in the Fe^{3+} penetration depth were observed for the 50 and 5.0 mM $FeCl_3$ solutions as
342 a result of stirring (see Figures S1–S12), which is fully consistent with the explanation that (i)
343 solution flow through the frit is extremely slow, (ii) convective transport as the result of stirring
344 only penetrates a few nanometers into the frit, and (iii) mass transport in the frit is dominated by
345 diffusion, whether the solution is stirred or not.

346 Similarly, the bottom panels of Figure 6 show three separate reference electrodes, each
347 filled with $FeCl_3$ ranging from 50 to 0.5 mM, exposed to solutions containing 2.5 M KSCN and
348 1.0 M KCl. With these electrodes, no downward stream of color was seen underneath the frit due
349 to the lower density of the $FeCl_3$ solutions that are contained in the frits. Diffusion of SCN^- into
350 some of the frits still occurred as the color penetrated into the frits containing 50 mM $FeCl_3$ and,

to a lesser extent, frits containing 5.0 mM $FeCl_3$. However, frits containing 0.5 mM $FeCl_3$ did not show any color change, indicating that partial ion screening occurred, as also indicated by the top panels of Figure 6. In addition, planar diffusion of Fe^{3+} from frits containing 50 and 5.0 mM $FeCl_3$ into the sample below formed a color that was much less intense than that within the frits. This is consistent with the expectation, based on ion concentrations and mobilities, that the flux of SCN^- from the sample into the frit is approximately two orders of magnitude larger than the Fe^{3+} flux out of the frit into the sample.

Figure 6 illustrates in a clear manner that porous junctions with low flow rates become significantly contaminated to a depth of several millimeters within the timescale of only one hour. This observation should be noted when performing long-term measurements with low flow-rate electrolyte bridges, and it demonstrates the drawbacks of storing salt bridges in solutions other than the electrolyte that they contain. Videos and images of this process are also included in the Supplementary Information, both for stirred and unstirred solutions.

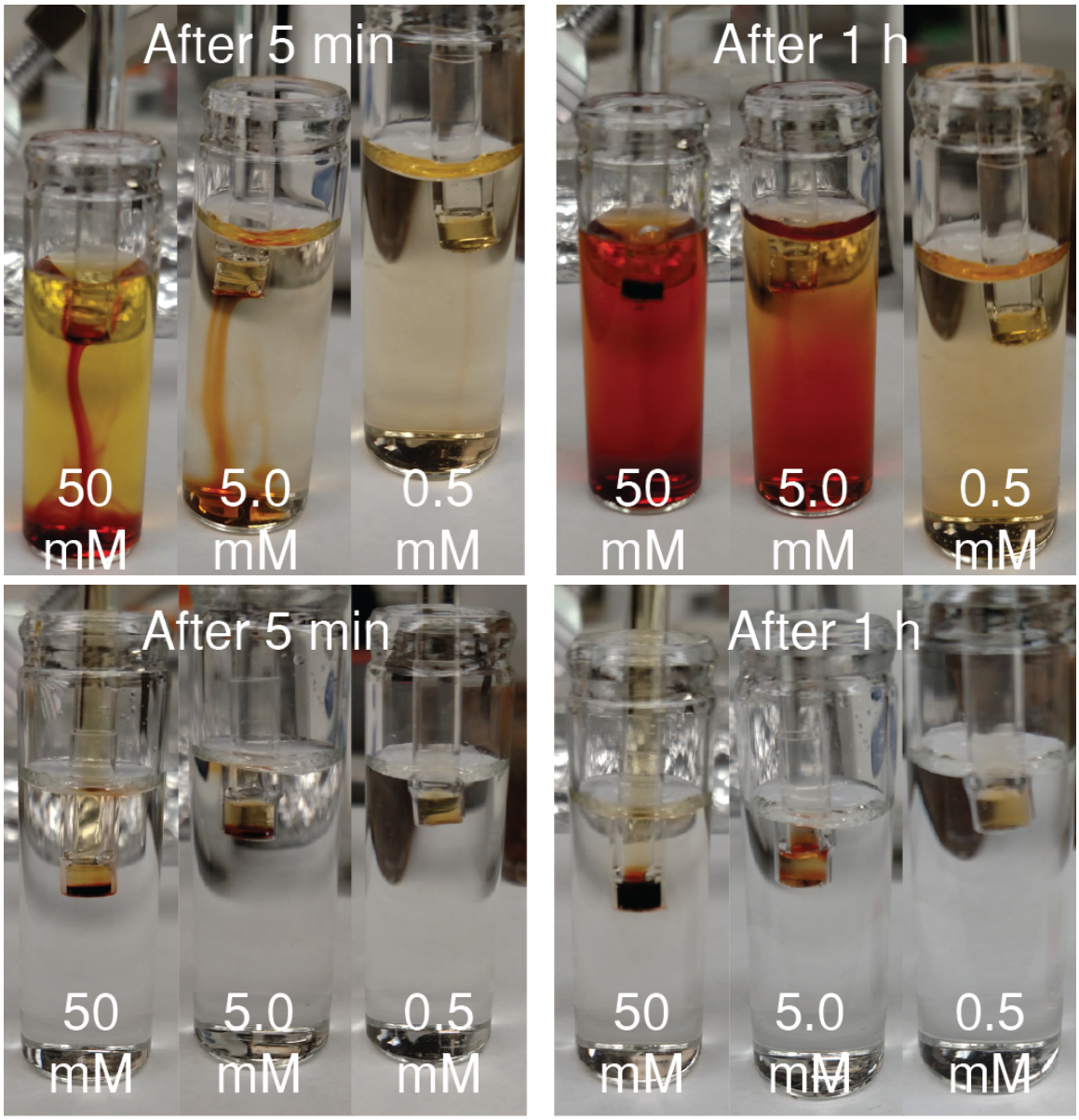

Figure 6. Top panel: Images of reference electrodes filled with 2.5 M KSCN/1.0 M KCl in contact with unstirred solutions of $FeCl_3$. Bottom panel: Images of reference electrodes filled with $FeCl_3$ in contact with unstirred solutions of 2.5 M KSCN/1.0 M KCl. The $FeCl_3$ concentrations and times of immersion of the reference electrodes into the sample solutions are indicated in the individual panels.

CONCLUSIONS

The potentials of reference electrodes with salt bridges contained in nanoporous glass frits have been shown in this work to depend on the rate with which the sample solutions are stirred. The convection that results from stirring causes mixing of sample solutions with bridge electrolyte within a layer of a few nanometers of the porous medium. When the sample is of considerably lower electrolyte strength than the bridge electrolyte, this convective mixing leads to deviations from the ideal behavior of salt bridges as it is predicted for a liquid-junction potential. This can be explained by an increase in the Debye length in the section of the frit that neighbors the sample solution, resulting in charge screening from the negatively charged frit surface. Reference potential measurements in solutions with low electrolyte strength (such as, e.g., rain water or water purified for industrial processing) will be particularly affected by charge screening, making accurate and reproducible measurements difficult. For example, a 60 mV change in reference potential would result in an order of magnitude error in the potentiometric measurement of a monovalent ion.

In addition, nanoporous frits through which bridge electrolyte flows with a rate that is smaller than the diffusion rate of species contained in the sample solution may over a period of only a few hours become contaminated with sample components and will lose bridge electrolyte near the interface of the sample and the porous frit. Users of reference electrodes with low flow rates should be aware that contaminants that have entered the bridge electrolyte can clog the salt bridge or will be released into samples during subsequent measurements. Moreover, temporary loss of bridge electrolyte caused by intermittent stirring can result in temporary charge screening at the frit surface and, therefore, drifts of the reference potential, which is easily misinterpreted as a slow response of the indicator electrode.

While all experiments presented in this work were performed with nanoporous glass frits, we anticipate similar effects for other nanoporous frits because materials to which no ions adsorb are elusive. Hydrophilic ions adsorb to polar materials, hydrophobic ions adsorb onto polymeric

materials without polar functional groups, and divalent cations such as Ca^{2+}, Mg^{2+} and many multivalent heavy metal ions bind to polyethers. To minimize sample-dependent phase boundary potentials at the salt bridge interface, frit material and pore size may be chosen with a view to the type of ions that are expected in the sample. Alternatively, as shown in this work, the flow rate of the bridge electrolyte into the sample must be high enough to avoid convective mass transport of sample into the frit, e.g., as a result of sample stirring.

ASSOCIATED CONTENT

Supporting Information.

Schematic of the experimental setup used to measure potentials at the interface of sample solutions and porous frits. Average potential of nanoporous frit reference electrodes in purified water as a function of stir rate. Images of reference electrodes filled with 2.5 M KSCN/1.0 M KCl in contact with stirred and unstirred solutions of 50, 5.0, and 0.5 mM $FeCl_3$ after 5 to 90 min. Time-lapse videos in mp4 format of reference electrodes filled with 2.5 M KSCN/1.0 M KCl in contact with stirred and unstirred solutions of 50, 5.0, and 0.5 mM $FeCl_3$.

AUTHOR INFORMATION

Corresponding Authors

*Philippe Buhlmann, buhlmann@umn.edu

ORCID

Philippe Bühlmann: 0000-0001-9302-4674.

Timothy P. Lodge: 0000-0001-5916-8834

Evan L. Anderson: 0000-0002-2506-1147

Notes

The authors declare no competing financial interest.

ACKNOWLEDGEMENTS

This work was supported partially by the National Science Foundation (CHE-1748148). E.L.A. thankfully acknowledges a Lester C. and Joan M. Krogh Endowed Fellowship, an ACS Division of Analytical Chemistry and Eastman Summer Fellowship, a Richard D. Amelar and Arthur S. Lodge Fellowship, and a Dissertation Fellowship from the Graduate School, University of Minnesota. The experiments were conducted at the Minnesota NMR Center (S10 OD021536).

REFERENCES

1. Bakker, E., Can calibration-free sensors be realized? *ACS Sens.* **2016,** *1*, 838-841.

2. Cuartero, M.; Bakker, E., Environmental water analysis with membrane electrodes. *Curr. Opin. Electrochem.* **2017,** *3*, 97-105.

3. Mousavi, M. P.; Saba, S. A.; Anderson, E. L.; Hillmyer, M. A.; Bühlmann, P., Avoiding errors in electrochemical measurements: Effect of frit material on the performance of reference electrodes with porous frit junctions. *Anal. Chem.* **2016,** *88*, 8706-8713.

4. Kakiuchi, T.; Yoshimatsu, T., A new salt bridge based on the hydrophobic room-temperature molten salt. *Bull. Chem. Soc. Jpn.* **2006,** *79*, 1017-1024.

5. Kakiuchi, T.; Yoshimatsu, T.; Nishi, N., New class of Ag/AgCl electrodes based on hydrophobic ionic liquid saturated with AgCl. *Anal. Chem.* **2007,** *79*, 7187-7191.

6. Hu, J.; Stein, A.; Bühlmann, P., Rational design of all-solid-state ion-selective electrodes and reference electrodes. *TrAC, Trends Anal. Chem.* **2016,** *76*, 102-114.

7. Kisiel, A.; Marcisz, H.; Michalska, A.; Maksymiuk, K., All-solid-state reference electrodes based on conducting polymers. *Analyst* **2005,** *130*, 1655-1662.

8. Cicmil, D.; Anastasova, S.; Kavanagh, A.; Diamond, D.; Mattinen, U.; Bobacka, J.; Lewenstam, A.; Radu, A., Ionic liquid-based, liquid-junction-free reference electrode. *Electroanalysis* **2011,** *23*, 1881-1890.

9. Zhang, T.; Lai, C. Z.; Fierke, M. A.; Stein, A.; Bühlmann, P., Advantages and limitations of reference electrodes with an ionic liquid junction and three-dimensionally ordered macroporous carbon as solid contact. *Anal. Chem.* **2012,** *84*, 7771-7778.

10. Zou, X. U.; Chen, L. D.; Lai, C.-Z.; Bühlmann, P., Ionic liquid reference electrodes with a well-controlled Co(II)/Co(III) redox buffer as solid contact. *Electroanalysis* **2015,** *27*, 602-608.

11. Chopade, S. A.; Anderson, E. L.; Schmidt, P. W.; Lodge, T. P.; Hillmyer, M. A.; Bühlmann, P., Self-supporting, hydrophobic, ionic liquid-based reference electrodes prepared by polymerization-induced microphase separation. *ACS Sens.* **2017,** *2*, 1498-1504.

12. Branch, S. D.; Lines, A. M.; Lynch, J.; Bello, J. M.; Heineman, W. R.; Bryan, S. A., Optically transparent thin-film electrode chip for spectroelectrochemical sensing. *Anal. Chem.* **2017,** *89*, 7324-7332.

13. Guinovart, T.; Crespo, G. A.; Rius, F. X.; Andrade, F. J., A reference electrode based on polyvinyl butyral (PVB) polymer for decentralized chemical measurements. *Anal. Chim. Acta* **2014,** *821*, 72-80.

14. Gao, W.; Emaminejad, S.; Nyein, H. Y. Y.; Challa, S.; Chen, K.; Peck, A.; Fahad, H. M.; Ota, H.; Shiraki, H.; Kiriya, D.; Lien, D. H.; Brooks, G. A.; Davis, R. W.; Javey, A., Fully integrated wearable sensor arrays for multiplexed in situ perspiration analysis. *Nature* **2016,** *529*, 509-514.

15. Lan, W. J.; Maxwell, E. J.; Parolo, C.; Bwambok, D. K.; Subramaniam, A. B.; Whitesides, G. M., Paper-based electroanalytical devices with an integrated, stable reference electrode. *Lab Chip* **2013,** *13*, 4103-4108.

16. Carano, M.; Colonna, B.; Echegoyen, L.; Le Derf, F.; Levillain, E.; Salle, M., Aqueous reference electrodes are unstable in organic media containing metal ions: A cautionary note to the supramolecular chemistry community. *Supramol. Chem.* **2003,** *15*, 83-85.

17. Dohner, R. E.; Wegmann, D.; Morf, W. E.; Simon, W., Reference electrode with free-flowing free-diffusion liquid junction. *Anal. Chem.* **1986,** *58*, 2585-2589.

18. Bard, A.; Faulkner, L., *Electrochemical methods: Fundamentals and applications*. John Wiley and Sons: Hoboken, New Jersey, 2001; Vol. 2.

19. Gorman, M.; Murphy, S. M. C., Liquid junction potential calculations. *J. Chem. Educ.* **1949,** *26*, 579.

20. Morf, W. E., Calculation of liquid-junction potentials and membrane potentials on the basis of the Planck theory. *Anal. Chem.* **1977,** *49*, 810-813.

21. Harper, H. W., Calculation of liquid junction potentials. *J. Phys. Chem.* **1985,** *89*, 1659-1664.

22. Morf, W. E., *The principles of ion-selective electrodes and of membrane transport*. Elsevier: New York, 1981.

23. Victoria, L.; Ortega, M. G.; Ibanez, J. A., Construction and evaluation of an inexpensive reference electrode with internal electrolyte in agar matrix. *J. Chem. Educ.* **1990,** *67*, 179.

24. Maurer, O.; Thieme, R. Apparatus for producing a pressure on the electrolytes in an electrode. DE 1,233,172, Jan. 26, 1967.

25. Gao, F.; Broadley, S.; Chen, T.-Y.; Payne, P. M.; Silverman, H., A stable ultra low flow reference electrode using a nanochannel glass array junction. *ECS Trans.* **2006,** *1*, 1-8.

26. Yonco, R. M.; Nagy, Z. Long life reference electrode. U.S. Patent 4,818,366. Jul. 30, 1989.

27. Crandall, E. D.; DeLong, J., A pressure- and flow-insensitive reference electrode liquid junction. *J. Appl. Physiol.* **1976,** *41*, 125-128.

28. Koopman, F.; Kunkler, J. L. Reference and glass electrodes capable of withstanding high pressures. U.S. Patent 3463717A. Aug. 26, 1969.

29. Schindler, J. G.; Riemann, W. Reference electrodes for electrochemical analytical instruments. DE 2,559,816. Sept. 21, 1978.

30. Sugano, K.; Katayama, T.; Koyama, M. Flow-through reference electrodes. JP 61,086,643. May 2, 1986.

31. Bakker, E.; Bühlmann, P.; Pretsch, E., The phase-boundary potential model. *Talanta* **2004,** *63*, 3-20.

32. Mousavi, M. P.; Bühlmann, P., Reference electrodes with salt bridges contained in nanoporous glass: An underappreciated source of error. *Anal. Chem.* **2013,** *85*, 8895-8901.

33. Meier, P. C., 2-parameter Debye–Hückel approximation for the evaluation of mean activity-coefficients of 109 electrolytes. *Anal. Chim. Acta* **1982,** *136*, 363-368.

34. Kirkwood, J. G.; Riseman, J., The intrinsic viscosities and diffusion constants of flexible macromolecules in solution. *J. Chem. Phys.* **1948,** *16*, 565-573.

35. Zimm, B. H., Dynamics of polymer molecules in dilute solution: Viscoelasticity, flow birefringence and dielectric loss. *J. Chem. Phys.* **1956,** *24*, 269-278.

36. Hiemenz, B. H.; Lodge, T. P., Introduction to polymer chemistry. CRC Press: Boca Raton, 2007; Vol. 2nd.

37. Bent, H. E.; French, C. L., The structure of ferric thiocyanate and its dissociation in aqueous solution. *J. Am. Chem. Soc.* **1941,** *63*, 568-572.

38. Dozier, W. D.; Drake, J. M.; Klafter, J., Self-diffusion of a molecule in porous vycor glass. *Phys. Rev. Lett.* **1986,** *56*, 197-200.

39. Dore, J. C.; Teixeira, J.; *Hydrogen-bonded Liquids*. North Atlantic Treaty Organization. Scientific Affairs Division. 1991

40. Oesch, U.; Simon, W., Lifetime of neutral carrier based ion-selective liquid-membrane electrodes. *Anal. Chem.* **1980,** *52*, 692-700.

41. Helfferich, F. G., *Ion exchange*. McGraw-Hill: New York, 1962.

42. Newton, M. R.; Bohaty, A. K.; White, H. S.; Zharov, I., Chemically modified opals as thin permselective nanoporous membranes. *J. Am. Chem. Soc.* **2005,** *127*, 7268-7269.

43. Wang, G.; Zhang, B.; Wayment, J. R.; Harris, J. M.; White, H. S., Electrostatic-gated transport in chemically modified glass nanopore electrodes. *J. Am. Chem. Soc.* **2006,** *128*, 7679-7686.

44. Lan, W. J.; Edwards, M. A.; Luo, L.; Perera, R. T.; Wu, X.; Martin, C. R.; White, H. S., Voltage-rectified current and fluid flow in conical nanopores. *Acc. Chem. Res.* **2016,** *49*, 2605-2613.

45. Morf, W. E.; Kahr, G.; Simon, W., Theoretical treatment of the selectivity and detection limit of silver compound membrane electrodes. *Anal. Chem.* **1974,** *46*, 1538-1543.

46. Dyke, M. V., *An album of fluid motion*. The Parabolic Press: Ann Arbor, Michigan, 1982.

47. Georgiadou, M.; Mohr, R.; Alkire, R. C., Local mass transport in two-dimensional cavities in laminar shear flow. *J. Electrochem. Soc.* **2000,** *147*, 3021.

532 48. Shen, C.; Floryan, J. M., Low reynolds number flow over cavities. *Phys. Fluids* **1985,** *28*,
533 3191.
534 49. Takematsu, M., Slow viscous flow past a cavity. *J. Phys. Soc. Jpn.* **1966,** *21*, 1816-1821.
535 50. Higdon, J. J. L., Stokes flow in arbitrary two-dimensional domains: Shear flow over ridges
536 and cavities. *J. Fluid Mech.* **2006,** *159*, 195.
537 51. Taneda, S., Visualization of separating stokes flows. *J. Phys. Soc. Jpn.* **1979,** *46*, 1935-
538 1942.
539 52. Koneshan, S.; Rasaiah, J. C.; Lynden-Bell, R. M.; Lee, S. H., Solvent structure, dynamics,
540 and ion mobility in aqueous solutions at 25 °C. *J. Phys. Chem. B* **1998,** *102*, 4193-4204.
541 53. Inzelt, G.; Lewenstam, A.; Scholz, F., *Handbook of reference electrodes*. Springer:
542 Heidelberg, Germany, 2013.
543 54. Lefrou, C.; Fabry, P.; Poignet, J., *Electrochemistry : The basics, with examples*. Springer
544 ed.; SpringerLink: New York, 2012.
545 55. Martínez Casillas, D. C.; Longinotti, M. P.; Bruno, M. M.; Vaca Chávez, F.; Acosta, R.
546 H.; Corti, H. R., Diffusion of water and electrolytes in mesoporous silica with a wide range of pore
547 sizes. *J. Phys. Chem. C* **2018,** *122*, 3638-3647.
548 56. Kuznetsova, A. S.; Volkova, A. V.; Ermakova, L. E.; Antropova, T. V., Iron(III) ion
549 adsorption on macroporous glass. *Glass Phys. Chem* **2018,** *44*, 41-46.
550
551

552 **TABLE OF CONTENTS GRAPHIC**

553

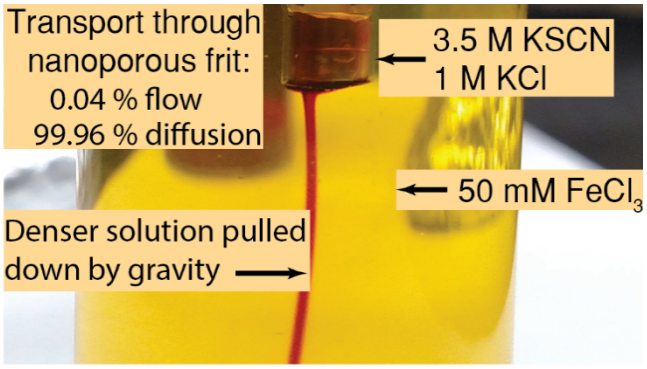

554